Majorana Zero Modes in the Lieb-Kitaev Model with Tunable Quantum Metric

Xingyao Guo,* Xinglei Ma,* Xuzhe Ying, and K. T. Law†
Department of Physics, Hong Kong University of Science and Technology, Clear Water Bay, Hong Kong, China

(Received 23 November 2024; revised 10 March 2025; accepted 30 June 2025; published 12 August 2025)

The relation between band topology and Majorana zero energy modes (MZMs) in topological superconductors had been well studied in the past decades. However, the relation between the quantum metric and MZMs has yet to be understood. In this Letter, we first construct a three band Lieb-like lattice model with an isolated flat band and tunable quantum metric. By introducing nearest neighbor equal spin pairing, we obtain the Lieb-Kitaev model which supports MZMs. When the Fermi energy is set within the flat band energy, the MZMs, which are supposed to be well localized at the ends of the 1D superconductor due to the flatness of the band, appear. On the contrary, we show both numerically and analytically that the localization length of the MZMs is controlled by a length scale defined by the quantum metric of the flat band, which we call the quantum metric length (QML). The QML can be several orders of magnitude longer than the conventional BCS superconducting coherence length. When the QML is comparable to the length of the superconductor, the two MZMs from the two ends of the superconductor can hybridize and induce ultra long range crossed Andreev reflections. This Letter unveils how the quantum metric can greatly influence the properties of MZMs through the QML, and the results can be generalized to other topological bound states.

DOI: 10.1103/l3c7-knqm

Introduction—Majorana zero energy modes (MZMs) are non-Abelian excitations in topological superconductors [1–21]. Due to the non-Abelian nature of MZMs and their ability to store quantum information which is immune to local perturbations [22–24], the study of MZMs has been one of the most important topics in condensed matter physics in the past few decades [25–28]. As first pointed out by Read and Green [1], two-dimensional $p+ip$ superconductors which are characterized by nontrivial Chern numbers support chiral Majorana edge modes. The Chern number is defined as the sum of the Berry curvature of occupied quasiparticle states of the Bogoliubov-de Gennes (BdG) Hamiltonian. Using a single band model with spinless p-wave pairing [Fig. 1(a)], Kitaev pointed out that one-dimensional topological superconductors support MZMs and the MZMs are localized at the two ends of the superconducting wires [2].

After the above seminal works [1,2], a large number of studies contributed to the experimental realization and detection of MZMs [29–38]. However, previous works were mostly focused on the topological aspects of MZMs, which are essentially connected to the Berry curvatures of the quasiparticle states. Interestingly, the Berry curvature is only one of the two aspects of the so-called quantum

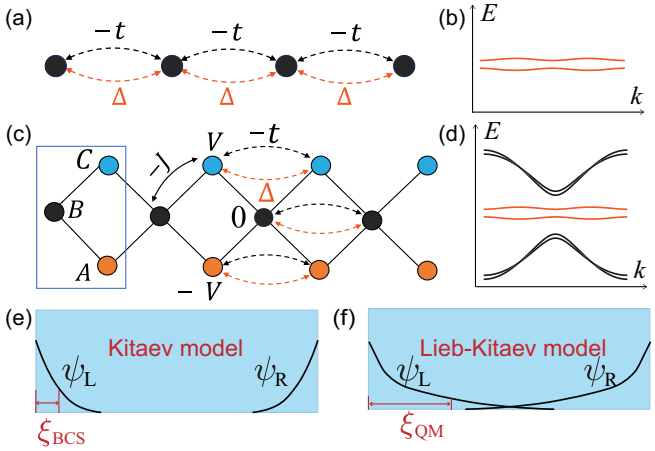

FIG. 1. (a),(c) Schematic illustrations of the real space single band Kitaev model (a) and the three band Lieb-Kitaev model (c). In (a), t denotes the nearest neighbor hopping and Δ is the nearest neighbor pairing. In (c), each unit cell contains three lattice sites A,B, and C, respectively. J, t, and Δ are the nearest neighbor hopping, the next nearest neighbor hopping, and the nearest neighbor pairing, respectively. (b),(d) Illustrations of the band structure of the Kitaev model (b) and the Lieb-Kitaev model (d). (e),(f) Illustrations of the Majorana wave functions ψ_L and ψ_R of the Kitaev model (e) and the Lieb-Kitaev model (f). The spread of $\psi_{L/R}$ is controlled by $\xi_{BCS} \approx at/\Delta$ in the Kitaev model and by the QML ξ_{QM} in the Lieb-Kitaev model, respectively.

*These authors contributed equally to this work.
†Contact author: phlaw@ust.hk

Published by the American Physical Society under the terms of the Creative Commons Attribution 4.0 International license. Further distribution of this work must maintain attribution to the author(s) and the published article's title, journal citation, and DOI.

geometry of the quantum states [39–41]. Given a Bloch state labeled by crystal momentum $\boldsymbol{k}$, we can construct the quantum geometry tensor $\mathfrak{G}(\boldsymbol{k}) = \mathcal{G}(\boldsymbol{k}) - i\mathcal{F}(\boldsymbol{k})/2$ [41]. Here, the real part $\mathcal{G}$ is the quantum metric tensor of the Bloch states and the imaginary part $\mathcal{F}$ is the Berry curvature. While the study of quantum metric effects has attracted much attention in recent years [42–61], the relation between the quantum metric and the properties of the topological bound states has yet to be understood. This Letter is devoted to understanding the connection between the quantum metric and the properties of the MZMs.

To study the quantum metric effects on MZMs, we introduce the Lieb-Kitaev model which supports MZMs and with tunable quantum metric. In the normal state, the model is a spinless Lieb-like lattice with three orbitals per unit cell [Fig. 1(c)]. This lattice structure results in a (nearly) flat band between the two dispersive bands in the energy spectrum [Fig. 2(a)]. Subsequently, we add the nearest neighbor intraorbital pairings to the Lieb-like lattice to create a p-wave superconductor with MZMs, when the chemical potential is within the flat band energy. The resulting Bogoliubov quasiparticle bands are schematically illustrated in Fig. 1(d). The Majorana wave functions are illustrated in Fig. 1(f).

There are three important results in this Letter. First, the quantum metric, which measures the quantum distance between two Bloch states [39,41], indeed sets a length scale in real space which we call the quantum metric length (QML) ξ_{QM} as defined in Eq. (3) [60,62]. The QML, defined as the average of the quantum metric over the Brillouin zone, governs the localization length as well as the quadratic spread of the Majorana wave functions for superconductors with (nearly) flat bands. Importantly, the QML is tunable, and it can be orders of magnitude longer than the lattice length scale as illustrated in Fig. 2(b). Second, in flat band topological superconductors with long QML, the two MZMs from the two ends of the topological superconductor can hybridize with each other over a long distance even though the conventional BCS superconducting coherence length ξ_{BCS} of the flat band superconductor is short. Here, $\xi_{\mathrm{BCS}} \approx at/\Delta$ where $2t$ is the bandwidth, Δ is the pairing amplitude of the flat band, and a is the lattice constant. Third, the hybridization of MZMs can result in long range nonlocal transport processes such as crossed Andreev reflections (CARs) when two metallic leads are connected to the two MZMs separately [7,12,63]. Remarkably, the CAR amplitudes can be comparable to the maximal theoretical value even when the separation of leads is several orders of magnitude longer than the ξ_{BCS} of the flat band.

Lieb-Kitaev model—In this section, we introduce the Lieb-Kitaev model for the realization of topological superconductors with tunable quantum metric. In the normal state of the Lieb-like lattice, the on-site energies of the (A, B, C) orbitals are $(-V, 0, V)$, respectively, as illustrated in Fig. 1(c). The nearest neighbor hopping amplitude is J. Additionally, a much smaller intraorbital hopping t is introduced [black dashed lines in Fig. 1(c)]. Accordingly, the Hamiltonian in the Bloch basis $\hat{\boldsymbol{c}}(k) = [\hat{c}_A(k), \hat{c}_B(k), \hat{c}_C(k)]^{\mathrm{T}}$ is written as

$$h(k) = [-2t\cos(ka) - \mu]\mathbb{I}_3 + \begin{pmatrix} -V & a_k & 0 \\ a_k^* & 0 & a_k^* \\ 0 & a_k & V \end{pmatrix}. \quad (1)$$

Here, μ is the chemical potential, $a_k = -J(1 + e^{ika})$ where a is the lattice constant, and $\mathbb{I}_3$ is the identity matrix. Figure 2(a) depicts the band structure of the model as defined in Eq. (1). We focus on the (nearly) flat band with dispersion $\epsilon_0 = -2t\cos(ka) - \mu$, where $2t$ is the bandwidth of the flat band. When $t = 0$, the band is exactly flat [blue line in Fig. 2(a)]. The flat band is separated from two dispersive bands by an energy gap $E_{\mathrm{g}} = |V|$. The eigenstates of the flat band are

$$u_0(k) = (a_k, V, -a_k)^T / \sqrt{4J^2[1 + \cos(ka)] + V^2}, \quad (2)$$

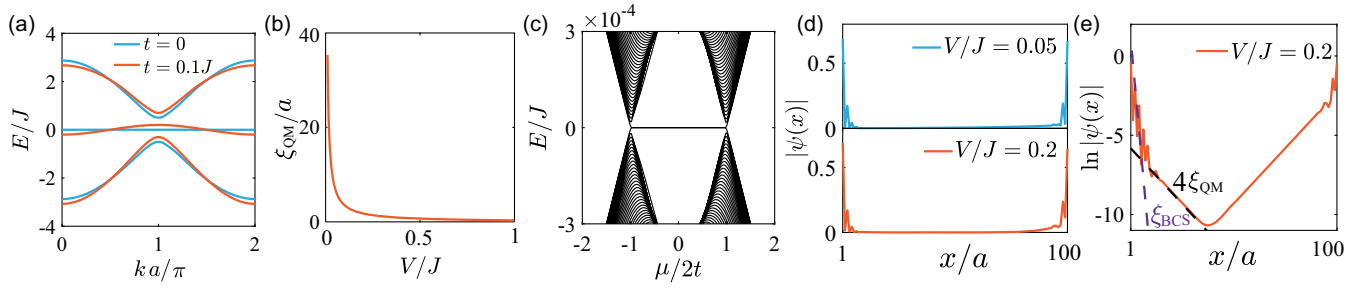

FIG. 2. (a) Normal state energy spectrum with $t = 0$ (blue line) and $t = 0.1J$ (orange line), respectively. $J = 1$ and $V = 0.2J$ are assumed in Eq. (1). (b) QML as a function of V/J. (c) Energy levels of a lattice model of H_{BDG} as a function of $\mu/2t$ with open boundary conditions. The parameters are $t = 3 \times 10^{-4}J$, $\Delta = 0.6t$, and $V = 0.2J$. The zero energy modes appear in the topological regime $|\mu| < 2t$. (d) Wave function amplitudes of MZMs with different V/J. The length of the superconductor $L = 100a$. The parameters are the same as in (c) except V/J. Chemical potential is set as $\mu = 0$. (e) $\ln|\psi(x)|$ is plotted for $|\psi(x)|$ in (d) with $V/J = 0.2$. The short distance localization length is controlled by ξ_{BCS} (dotted purple line) and the long distance localization length (dotted black line) is controlled by $4\xi_{\mathrm{QM}}$. The numerical results are in perfect agreement with Eq. (7).

which is essential for computing the quantum metric as well as constructing the Majorana wave functions as shown below.

The quantum metric of a state with momentum k of the flat band is defined as $\mathcal{G}(k) = \langle \partial_k u_0(k)|[\mathbb{I} - |u_0(k)\rangle\langle u_0(k)|]|\partial_k u_0(k)\rangle$ which has the dimension of length-squared. The QML ξ_{QM} is defined as the Brillouin zone averaged quantum metric:

$$\xi_{\mathrm{QM}} \equiv \int_0^{2\pi/a} \mathcal{G}(k)\frac{dk}{2\pi} \xrightarrow{\frac{V}{J}\to 0} \frac{\sqrt{2}}{4}\frac{J}{V}a. \tag{3}$$

The length scale ξ_{QM} is particularly important for exactly flat bands with $t = 0$ and vanishing Fermi velocity. In this case, the conventional length scales such as the Fermi wavelength is not well defined, and the BCS coherence length $\xi_{\mathrm{BCS}} \approx at/\Delta$ is zero for flat bands. As we show below, the QML ξ_{QM} is still a dominant length scale which governs the spread of the Majorana wave functions in topological superconductors when ξ_{QM} is longer than ξ_{BCS}. Moreover, for the Lieb-like lattice, the ξ_{QM} is tunable by changing V/J. Figure 2(b) shows that ξ_{QM} is divergent when V/J approaches 0. With the tunable QML, the Lieb-like lattice is an ideal model for studying the interplay between the topology and quantum metric.

To realize MZMs, we introduce intraorbital pairing with amplitude Δ between sites from adjacent unit cells, indicated by the red dashed line in Fig. 1(c). The resulting BdG Hamiltonian of the Lieb-Kitaev model is

$$H_{\mathrm{BdG}} = \sum_k \hat{\Psi}^\dagger(k)\begin{pmatrix} h(k) & -i2\Delta\sin(ka)\mathbb{I}_3 \\ i2\Delta\sin(ka)\mathbb{I}_3 & -h^*(-k)\end{pmatrix}\hat{\Psi}(k), \tag{4}$$

where $\hat{\Psi}(k) = [\hat{\boldsymbol{c}}(k), \hat{\boldsymbol{c}}^\dagger(-k)]^{\mathrm{T}}$. Figure 2(c) shows the energy levels of a finite size system with open boundary conditions within the energy window $E \in [-t, t]$. We observe that zero energy modes exist when the chemical potential lies in the region $|\mu| < 2t$. The topological phase is characterized by the Z2 number $Q = \mathrm{sign}(\mathrm{Pf}[i\tilde{H}(k = 0)]\mathrm{Pf}\{i\tilde{H}[k = (\pi/a)]\}$ [2,64]. As shown in Supplemental Material [65], in cases of $|\mu| < 2t$, we have $\mathcal{Q} = -1$, which corresponds to the topologically nontrivial regime.

Figure 2(d) depicts the Majorana wave functions of the models with two different values of V/J and $\Delta = 0.6t$ such that the band is extremely flat. With a larger quantum metric (smaller V/J), the Majorana wave functions can penetrate deeper into the bulk of the flat band superconductor. The localization length of the Majorana wave functions is indeed much longer than t/Δ, which is different from the single band Kitaev model. The asymmetry of the Majorana wave functions from the two ends of the superconductor originates from the inversion symmetry breaking of the underlying lattice. To quantify the spread of the Majorana wave functions, we plot $\ln|\psi(x)|$ versus position x in Fig. 2(e). Here, $\psi(x)$ is the wave function of the fermionic mode which includes the Majorana wave functions from the left and the right boundaries. For the Majorana modes of the left boundary, for example, there are two different decay modes in short and long distances as shown in Fig. 2(e). At a relative short distance away from the left boundary, the Majorana wave function decays as $e^{-x/\xi_{\mathrm{BCS}}}$ [purple dashed line in Fig. 2(e)], where $\xi_{\mathrm{BCS}} = -2a/\ln[(t-\Delta)/(t+\Delta)]$ [66]. For $t \gg \Delta$, we have $\xi_{\mathrm{BCS}} \approx at/\Delta$, and we call this length the BCS coherence length. However, at larger x, a different decay behavior takes over, and the wave function decays as $e^{-x/4\xi_{\mathrm{QM}}}$ [black dashed line in Fig. 2(e)], where ξ_{QM} is the QML defined in Eq. (3). In the next section, we will show analytically how the QML emerges in the Majorana wave functions.

Wave functions, localization length, and quadratic spread of MZMs—To begin with, we consider the multiband Hamiltonian $H = H_0 + H_1$, where H_0 is the lattice representation of Eq. (4) with N sites and a periodic boundary condition. The perturbation H_1 removes the hopping and pairing between the first site 1 and the last site N of H_0, and the addition of H_1 results in a Hamiltonian with an open boundary condition [67]. For $V \gg t \simeq \Delta$ and $|\mu| < 2t$, the two isolated quasiparticle bands labeled by $n = \pm$ respectively are close to the Fermi energy and far away from other bands. The eigenstates of the $n = \pm$ bands are denoted by $g_n(k)$, where $H_{\mathrm{BdG}}(k)g_n(k) = \varepsilon_n(k)g_n(k)$. The eigenstate $\psi(x)$ which contains both the left Majorana mode $\psi_{\mathrm{L}}(x)$ and the right Majorana mode $\psi_{\mathrm{R}}(x)$ can be expressed in a self-consistent way as

$$\begin{aligned}\psi(x) &= \psi_{\mathrm{L}}(x) + i\psi_{\mathrm{R}}(x) \\ &= -G^p(x, Na; E)U_{01}\psi(a) - G^p(x, a; E)U_{01}^\dagger\psi(Na),\end{aligned} \tag{5}$$

where

$$G^p(x_j, x_{j'}; E) = \frac{1}{N}\sum_{n=\pm}\sum_k \frac{g_n(k)g_n^\dagger(k)}{E - \varepsilon_n(k)}e^{ik(x_j - x_{j'})} \tag{6}$$

is the projected Green function, where j/j' is the site index and $E = 0$ for the MZMs. The operator U_{01} is the coupling matrix between adjacent unit cells. The details of the calculations for the Majorana wave functions are presented in Supplemental Material [65].

Away from the left boundary (the first site) and by setting $\mu = 0$ for simplicity, the left Majorana wave function can be written as

$$\psi_{\mathrm{L}}(x_j) = A_{\mathrm{L}}^{\mathrm{QM}} e^{-\frac{(j-1)a}{4\xi_{\mathrm{QM}}}} + A_{\mathrm{L}}^{\mathrm{BCS}} e^{-\frac{(j-1)a}{\xi_{\mathrm{BCS}}}}. \tag{7}$$

Here, $A_{\mathrm{L}}^{\mathrm{QM}}$ and $A_{\mathrm{L}}^{\mathrm{BCS}}$ are the amplitudes of two parts of the wave function with different localization lengths $4\xi_{\mathrm{QM}}$ and ξ_{BCS}, respectively. The localization lengths are determined by the poles of $g_n(k)g_n^{\dagger}(k)/\varepsilon_n(k)$ in the complex plane. Physically, $\xi_{\mathrm{BCS}} = -2a/\ln[(t-\Delta)/(t+\Delta)]$ originates from the dispersion of quasiparticle bands $\varepsilon_{\pm}(k)$. This decay length is the same as the one in the single band Kitaev model with bandwidth $2t$ and pairing potential Δ [66]. Importantly, an extra pole of the Bloch wave functions gives rise to a decay length of $4\xi_{\mathrm{QM}}$ for the $A_{\mathrm{L}}^{\mathrm{QM}}$ component of the wave function. When $4\xi_{\mathrm{QM}} \gg \xi_{\mathrm{BCS}}$, the QML ξ_{QM} dominates the long range behavior of the Majorana wave function. The $A_{\mathrm{L}}^{\mathrm{BCS}}$ component has different amplitudes for the even or odd lattice sites, which explains the oscillation of MZMs' wave function as a function of lattice site. A similar expression for the wave function localized near the right boundary (the Nth site) $\psi_{\mathrm{R}}(x_j)$ is shown in Supplemental Material [65]. To compare the analytical results with the numerical results, the long distance localization length of MZMs ξ is extracted numerically (orange squared line), and it matches the analytical values of $4\xi_{\mathrm{QM}}$ (blue starred line) perfectly, as shown in Fig. 3(a).

Besides the localization length, the spread of a wave function can also be characterized by the quadratic spread which was used to measure the size of Wannier states [68]. The quadratic spread of the right Majorana can be evaluated as $\mathcal{QS}_{\mathrm{R}} \equiv \sum_{x=a}^{Na}(x-x_{\mathrm{R}})^2|\gamma_{\mathrm{R}}(x)|^2$, and x_{R} is the position of the right boundary. In the limit of small V/J, vanishing ξ_{BCS} with $t \approx \Delta$, and $\mu = 0$, to order $\mathcal{O}(V/J)$, we have

$$\mathcal{QS}_{\mathrm{R}} = \frac{a}{2\pi}\int_0^{2\pi/a} \mathcal{G}(k)dk = a\xi_{\mathrm{QM}}. \tag{8}$$

The analytical results are also in agreement with the numerical results as shown in Fig. 3(b). This is one of the key result of this Letter as it connects the quantum metric with the spread of the Majorana wave functions. The details of the derivation for Eq. (8) are given in Supplemental Material [65].

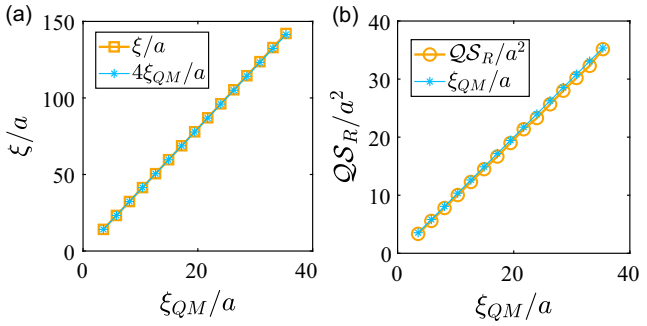

FIG. 3. (a) Comparison between the localization length of a MZM extracted numerically ξ and $4\xi_{\mathrm{QM}}$. (b) Quadratic spread $\mathcal{QS}$ of MZMs as a function of QML ξ_{QM}. The results are in agreement with Eq. (8). The parameters of the lattice model for both figures are $\mu = 0$, $t = 5\times10^{-4}J$, $\Delta = 4.95\times10^{-4}J$, and $V/J \in [0.01, 0.1]$.

Long range crossed Andreev reflection—In this section, we show that a long quantum metric length can induce long range nonlocal transport when two leads are coupled to the two MZMs separately. In particular, the CAR probability can nearly reach the maximal theoretical value even though the separation of the two leads is several orders of magnitude longer than the conventional localization length of the Majorana modes ξ_{BCS} in the one band Kitaev model.

Considering a device shown in Fig. 4(a), two normal metal leads are attached to two sides of the topological superconductor. A CAR process happens when an incoming electron from one lead is reflected as a hole in the other lead, leading to the formation of a Cooper pair in the grounded superconductor [7,12,63]. Due to the quantum metric induced spread of the Majorana modes as discussed above, the coupling between Majorana modes can be significant in a long topological superconducting wire. We expect that the coupled Majorana modes can mediate long range CARs as shown below.

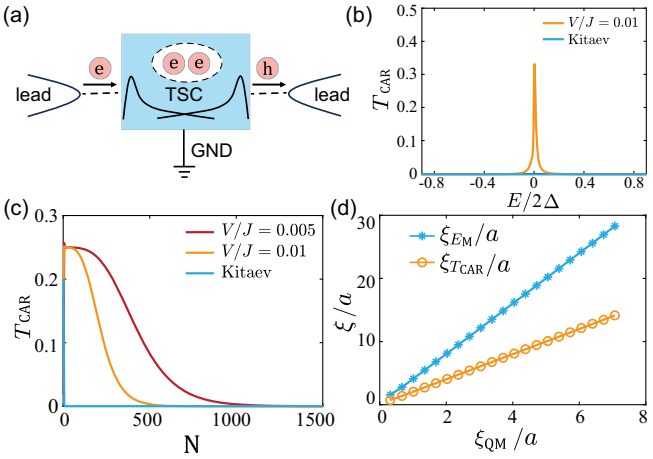

FIG. 4. (a) Schematic plot of a normal lead-topological superconductor (TSC)-normal lead device. Two leads couple to the two MZMs separately. In a CAR process, an electron from the left lead is reflected as a hole in the other lead. (b) CAR probability versus bias voltage $E =$ eV for the single band Kitaev model (blue line) and the Lieb-Kitaev model (yellow line). Parameters $J = 1$, $t = 1\times10^{-4}J$, $\Delta = 0.8t$, $\mu = 0.2t$, and $L = 100a$. $V/J = 0.01$ is set for the Lieb-Kitaev model. The same μ, t, and Δ are set for the single band Kitaev model. (c) CAR probability at zero bias $E = 0$ versus device length $L = Na$ for the Kitaev model (blue line) and the Lieb-Kitaev model with $V/J = 0.005$ (red line) and $V/J = 0.01$ (yellow line), respectively. (d) The long distance behavior of the hybridization energy E_{M} of the MZMs and the CAR probability T_{CAR} as a function of the length of the superconductor can be written as $E_{\mathrm{M}} \propto e^{-Na/\xi_{E_{\mathrm{M}}}}$ and $T_{\mathrm{CAR}} \propto e^{-Na/\xi_{T_{\mathrm{CAR}}}}$, respectively. Here, we show that $\xi_{E_{\mathrm{M}}} = 4\xi_{\mathrm{QM}}$ and $\xi_{T_{\mathrm{CAR}}} = 2\xi_{\mathrm{QM}}$. The parameters in (c) and (d) are the same as in (b) except L.

To be more specific, we perform recursive Green function calculations [69] to study the CAR probability T_{CAR} for both the single band Kitaev model and the Lieb-Kitaev model. The blue line in Fig. 4(c) shows that the CAR signal only survives in a short wire with a few tens of lattice sites for the single band Kitaev model [Fig. 1(a)]. The T_{CAR} diminishes quickly once the length of the superconductor increases as the MZMs cannot couple to each other due to the short localization lengths of the MZMs in the single band Kitaev model ξ_{BCS}.

In sharp contrast, as indicated by the red and yellow lines in Figs. 4(b) and 4(c), the CAR probability is dramatically enhanced in the Lieb-Kitaev model with large quantum metric. The T_{CAR} is most significant at low bias, as shown in Fig. 4(b). When the energy of the incoming electron is close to the energy of the fermionic mode formed by the hybrization of the MZMs, a large CAR probability, which is near the maximal theoretical value of 0.5, is possible [7]. Figure 4(c) depicts T_{CAR} versus the length of the superconductor at zero bias (red and yellow lines). We find that T_{CAR} can be large when the separation of the leads is comparable to the QML even when the QML is several orders of magnitude longer than at/Δ. It is striking that the CAR amplitude remains finite up to thousands of sites in cases of larger QML [red line in Fig. 4(c)] when $t/\Delta \approx 1$.

A more careful analysis shows that, at low voltage bias, the CAR probability is closely related to the coupling between the two MZMs. The strength of coupling between the MZMs is characterized by the hydridization energy E_{M}. As shown in Fig. 4(d), we found that the hydridization energy is proportional to the length of the topological superconductor such that $E_{\mathrm{M}} \propto e^{-Na/4\xi_{\mathrm{QM}}}$. Accordingly, the CAR probability can be expressed as $T_{\mathrm{CAR}} \propto e^{-Na/2\xi_{\mathrm{QM}}}$ [yellow line in Fig. 4(d)].

Discussion—In this Letter, we construct the Lieb-Kitaev model to study the effect of quantum metric on MZMs. It is shown that the localization length as well as the quadratic spread of the Majorana wave functions are controlled by the QML in a flat band topological superconductor. The two MZMs can couple to each other as long as the QML is comparable to the length of the flat band topological superconductor. The coupling of MZMs can induce long range CARs when two leads are coupled to the two ends of the topological superconductors. It is important to note that the Lieb-Kitaev model proposed only involves the nearest neighbor hopping and pairing. Therefore, quasi-one-dimensional moiré materials, which can be described by a Lieb-like lattice [70] in the normal state, can possibly be used to realize the Lieb-Kitaev model. A spinful Lieb-Kitaev model is introduced in Supplemental Material [65] for the discussion of possible experimental realization. The effect of QML in a two-dimensional model is also discussed [65]. As shown by Eq. (6) and in Sec. I of Supplemental Material [65], the dependence of the Majorana wave function on the QML is indeed very general for topological superconductors with isolated flat bands, and the validity of the conclusions of this Letter goes beyond the Lieb-Kitaev model. Importantly, the QML is defined by the wave functions of the normal state. Therefore, the conclusions of this Letter can be generalized to describe topological bound states in other topological materials.

Acknowledgments—We thank Shuai Chen, Adrian Po, and Bohm-Jung Yang for inspiring discussions. K. T. L. acknowledges the support of the Ministry of Science and Technology, China, and Hong Kong Research Grant Council through Grants No. MOST23SC01-A, No. 2020YFA0309600, No. RFS2021-6S03, No. C6025-19G, No. C6053-23G, No. AoE/P-701/20, No. 16310520, No. 16310219, No. 16307622, No. 16311424, and No. 16309223.

[1] N. Read and D. Green, Phys. Rev. B **61**, 10267 (2000).
[2] A. Y. Kitaev, Phys. Usp. **44**, 131 (2001).
[3] D. A. Ivanov, Phys. Rev. Lett. **86**, 268 (2001).
[4] M. Stone and S.-B. Chung, Phys. Rev. B **73**, 014505 (2006).
[5] L. Fu and C. L. Kane, Phys. Rev. Lett. **100**, 096407 (2008).
[6] S. Fujimoto, Phys. Rev. B **77**, 220501(R) (2008).
[7] J. Nilsson, A. R. Akhmerov, and C. W. J. Beenakker, Phys. Rev. Lett. **101**, 120403 (2008).
[8] L. Fu and C. L. Kane, Phys. Rev. B **79**, 161408(R) (2009).
[9] L. Fu and C. L. Kane, Phys. Rev. Lett. **102**, 216403 (2009).
[10] A. R. Akhmerov, J. Nilsson, and C. W. J. Beenakker, Phys. Rev. Lett. **102**, 216404 (2009).
[11] M. Sato, Y. Takahashi, and S. Fujimoto, Phys. Rev. Lett. **103**, 020401 (2009).
[12] K. T. Law, P. A. Lee, and T. K. Ng, Phys. Rev. Lett. **103**, 237001 (2009).
[13] J. D. Sau, R. M. Lutchyn, S. Tewari, and S. Das Sarma, Phys. Rev. Lett. **104**, 040502 (2010).
[14] J. Alicea, Phys. Rev. B **81**, 125318 (2010).
[15] R. M. Lutchyn, J. D. Sau, and S. Das Sarma, Phys. Rev. Lett. **105**, 077001 (2010).
[16] Y. Oreg, G. Refael, and F. von Oppen, Phys. Rev. Lett. **105**, 177002 (2010).
[17] K. Flensberg, Phys. Rev. B **82**, 180516(R) (2010).
[18] A. C. Potter and P. A. Lee, Phys. Rev. Lett. **105**, 227003 (2010).
[19] J. Alicea, Y. Oreg, G. Refael, F. von Oppen, and M. P. A. Fisher, Nat. Phys. **7**, 412 (2010).
[20] A. Cook and M. Franz, Phys. Rev. B **84**, 201105(R) (2011).
[21] J. J. He, T. K. Ng, P. A. Lee, and K. T. Law, Phys. Rev. Lett. **112**, 037001 (2014).
[22] A. Kitaev, Ann. Phys. (Amsterdam) **303**, 2 (2003).
[23] C. Nayak, S. H. Simon, A. Stern, M. Freedman, and S. Das Sarma, Rev. Mod. Phys. **80**, 1083 (2008).
[24] D. Aasen, M. Hell, R. V. Mishmash, A. Higginbotham, J. Danon, M. Leijnse, T. S. Jespersen, J. A. Folk, C. M. Marcus, K. Flensberg, and J. Alicea, Phys. Rev. X **6**, 031016 (2016).
[25] M. Z. Hasan and C. L. Kane, Rev. Mod. Phys. **82**, 3045 (2010).
[26] X.-L. Qi and S.-C. Zhang, Rev. Mod. Phys. **83**, 1057 (2011).

[27] J. Alicea, Rep. Prog. Phys. **75**, 076501 (2012).
[28] C. Beenakker, Annu. Rev. Condens. Matter Phys. **4**, 113 (2013).
[29] V. Mourik, K. Zuo, S. M. Frolov, S. R. Plissard, E. P. A. M. Bakkers, and L. P. Kouwenhoven, Science **336**, 1003 (2012).
[30] L. P. Rokhinson, X. Liu, and J. K. Furdyna, Nat. Phys. **8**, 795 (2012).
[31] A. Das, Y. Ronen, Y. Most, Y. Oreg, M. Heiblum, and H. Shtrikman, Nat. Phys. **8**, 887 (2012).
[32] M. T. Deng, C. L. Yu, G. Y. Huang, M. Larsson, P. Caroff, and H. Q. Xu, Nano Lett. **12**, 6414 (2012).
[33] S. Nadj-Perge, I. K. Drozdov, J. Li, H. Chen, S. Jeon, J. Seo, A. H. MacDonald, B. A. Bernevig, and A. Yazdani, Science **346**, 602 (2014).
[34] S. M. Albrecht, A. P. Higginbotham, M. Madsen, F. Kuemmeth, T. S. Jespersen, J. Nygård, P. Krogstrup, and C. M. Marcus, Nature (London) **531**, 206 (2016).
[35] B. Jäck, Y. Xie, J. Li, S. Jeon, B. A. Bernevig, and A. Yazdani, Science **364**, 1255 (2019).
[36] A. Fornieri, A. M. Whiticar, F. Setiawan, E. Portols, A. C. C. Drachmann, A. Keselman, S. Gronin, C. Thomas, T. Wang, R. Kallaher, G. C. Gardner, E. Berg, M. J. Manfra, A. Stern, C. M. Marcus, and F. Nichele, Nature (London) **569**, 89 (2019).
[37] H. Ren, F. Pientka, S. Hart, A. T. Pierce, M. Kosowsky, L. Lunczer, R. Schlereth, B. Scharf, E. M. Hankiewicz, L. W. Molenkamp, B. I. Halperin, and A. Yacoby, Nature (London) **569**, 93 (2019).
[38] D. Wang, L. Kong, P. Fan, H. Chen, S. Zhu, W. Liu, L. Cao, Y. Sun, S. Du, J. Schneeloch, R. Zhong, G. Gu, L. Fu, H. Ding, and H.-J. Gao, Science **362**, 333 (2018).
[39] J. P. Provost and G. Vallee, Commun. Math. Phys. **76**, 289 (1980).
[40] M. V. Berry, Proc. R. Soc. A **392**, 45 (1984).
[41] R. Resta, Eur. Phys. J. B **79**, 121 (2010).
[42] F. D. M. Haldane, Phys. Rev. Lett. **107**, 116801 (2011).
[43] S. A. Parameswaran, R. Roy, and S. L. Sondhi, C.R. Phys. **14**, 816 (2013).
[44] T. Neupert, C. Chamon, and C. Mudry, Phys. Rev. B **87**, 245103 (2013).
[45] Y. Gao, S. A. Yang, and Q. Niu, Phys. Rev. Lett. **112**, 166601 (2014).
[46] R. Roy, Phys. Rev. B **90**, 165139 (2014).
[47] S. Peotta and P. Törmä, Nat. Commun. **6**, 8944 (2015).
[48] A. Julku, S. Peotta, T. I. Vanhala, D.-H. Kim, and P. Törmä, Phys. Rev. Lett. **117**, 045303 (2016).
[49] L. Liang, T. I. Vanhala, S. Peotta, T. Siro, A. Harju, and P. Törmä, Phys. Rev. B **95**, 024515 (2017).
[50] M. Iskin, Phys. Rev. A **97**, 033625 (2018).
[51] J. S. Hofmann, E. Berg, and D. Chowdhury, Phys. Rev. B **102**, 201112(R) (2020).
[52] N. Verma, T. Hazra, and M. Randeria, Proc. Natl. Acad. Sci. U.S.A. **118**, e2106744118 (2021).
[53] V. Kozii, A. Avdoshkin, S. Zhong, and J. E. Moore, Phys. Rev. Lett. **126**, 156602 (2021).
[54] J. Ahn and N. Nagaosa, Phys. Rev. B **104**, L100501 (2021).
[55] A. Julku, G. M. Bruun, and P. Törmä, Phys. Rev. Lett. **127**, 170404 (2021).
[56] W. Chen and W. Huang, Phys. Rev. Res. **3**, L042018 (2021).
[57] J. Herzog-Arbeitman, V. Peri, F. Schindler, S. D. Huber, and B. A. Bernevig, Phys. Rev. Lett. **128**, 087002 (2022).
[58] J. Ahn, G.-Y. Guo, N. Nagaosa, and A. Vishwanath, Nat. Phys. **18**, 290 (2022).
[59] J. S. Hofmann, E. Berg, and D. Chowdhury, Phys. Rev. Lett. **130**, 226001 (2023).
[60] S. A. Chen and K. T. Law, Phys. Rev. Lett. **132**, 026002 (2024).
[61] T. Kitamura, A. Daido, and Y. Yanase, Phys. Rev. Lett. **132**, 036001 (2024).
[62] J.-X. Hu, S. A. Chen, and K. T. Law, Commun. Phys. **8**, 20 (2025).
[63] J. Liu, F.-C. Zhang, and K. T. Law, Phys. Rev. B **88**, 064509 (2013).
[64] A. P. Schnyder, S. Ryu, A. Furusaki, and A. W. W. Ludwig, Phys. Rev. B **78**, 195125 (2008).
[65] See Supplemental Material at http://link.aps.org/supplemental/10.1103/l3c7-knqm for (I) general relations between quantum metric and Majorana wavefunctions, (II) MZMs in the Lieb-Kitaev model, (III) the universal role of the quantum metric length, and (IV) length dependence of the crossed Andreev reflection probability.
[66] N. Leumer, M. Marganska, B. Muralidharan, and M. Grifoni, J. Phys. Condens. Matter **32**, 445502 (2020).
[67] R. S. K. Mong and V. Shivamoggi, Phys. Rev. B **83**, 125109 (2011).
[68] N. Marzari and D. Vanderbilt, Phys. Rev. B **56**, 12847 (1997).
[69] S. Datta, Non-equilibrium Green's function formalism, in *Electronic Transport in Mesoscopic Systems* (Cambridge University Press, Cambridge, England, 1995), pp. 293–342.
[70] H. C. Po, L. Zou, T. Senthil, and A. Vishwanath, Phys. Rev. B **99**, 195455 (2019).